Journal of proteome research

Article

Cite This: J. Proteome Res. 2018, 17, 1415−1425

pubs.acs.org/jpr

Deletion of Adipose Triglyceride Lipase Links Triacylglycerol Accumulation to a More-Aggressive Phenotype in A549 Lung Carcinoma Cells

Tamara Tomin,[†,‡] Katarina Fritz,[†,‡,#] Juergen Gindlhuber,[†,‡] Linda Waldherr,[†,‡] Bettina Pucher,[‡,§] Gerhard G. Thallinger,[‡,§] Daniel K. Nomura,[∥,⊥] Matthias Schittmayer,[†,‡] and Ruth Birner-Gruenberger*[,†,‡]

[†]Research Unit Functional Proteomics and Metabolic Pathways, Institute of Pathology, Medical University of Graz, 8010 Graz, Austria

[‡]Omics Center Graz, BioTechMed-Graz, 8010 Graz, Austria

[§]Institute of Computational Biotechnology, Graz University of Technology, 8010 Graz, Austria

[∥]Department of Chemistry, Molecular, and Cell Biology and [⊥]Department of Nutritional Sciences and Toxicology, University of California, Berkeley, California 94720, United States

Supporting Information

ABSTRACT: Adipose triglyceride lipase (ATGL) catalyzes the rate limiting step in triacylglycerol breakdown in adipocytes but is expressed in most tissues. The enzyme was shown to be lost in many human tumors, and its loss may play a role in early stages of cancer development. Here, we report that loss of ATGL supports a more-aggressive cancer phenotype in a model system in which ATGL was deleted in A549 lung cancer cells by CRISPR/Cas9. We observed that loss of ATGL led to triacylglycerol accumulation in lipid droplets and higher levels of cellular phospholipid and bioactive lipid species (lyso- and ether-phospholipids). Label-free quantitative proteomics revealed elevated expression of the pro-oncogene SRC kinase in ATGL depleted cells, which was also found on mRNA level and confirmed on protein level by Western blot. Consistently, higher expression of phosphorylated (active) SRC (Y416 phospho-SRC) was observed in ATGL-KO cells. Cells depleted of ATGL migrated faster, which was dependent on SRC kinase activity. We propose that loss of ATGL may thus increase cancer aggressiveness by activation of pro-oncogenic signaling via SRC kinase and increased levels of bioactive lipids.

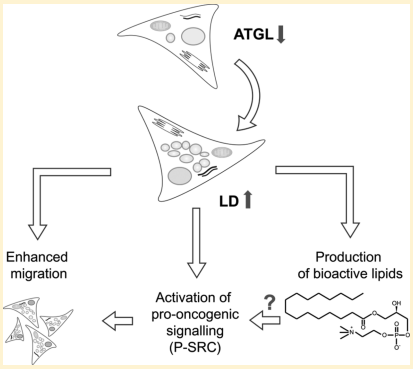

KEYWORDS: *ATGL, SRC, cancer, migration, lipid droplet, triacylglycerol, A549 lung carcinoma cells*

INTRODUCTION

Metabolic switching is one of the main hallmarks of malignant transformation.[1] While the increased uptake of glucose and the Warburg effect are well-known metabolic changes occurring in cancer cells, changes in lipid metabolism have attracted more attention recently.[2] Lipids, in addition to their most prominent nutritional and structural roles, can act as signaling molecules and influence proliferation, cell cycle, migration, and invasiveness of cancer cells. To sustain their fast growth, many cancer types alter their metabolism to meet higher energy requirements.[3] In lipid metabolism, this is usually manifested through increased uptake of dietary lipids[4] and enhanced de novo lipogenesis.[5] Such lipid-rich cancer cells eventually have to store excess lipids in the form of lipid droplets (LDs).[4] LDs are specialized organelles that are mainly composed of neutral lipids, triacylglycerol (TG), and sterolesters and are surrounded by an amphipathic layer of phospholipids and proteins.[6,7] A small number of LDs is present in most mammalian cells, and the highest concentration of LDs is found in adipocytes.[8] However, it has been reported that LD content increases dramatically in certain cancer types in comparison to surrounding normal tissue.[9] Evidence that accumulation of neutral lipids plays an important role in tumorigenesis can be found in hepatocellular carcinoma (HCC), in which the nonalcoholic fatty liver phenotype highly increases the probability of HCC.[10] High lipid content has been reported to drive metastatic potential and facilitate spheroid formation of different cancer cells exposed to hypoxia,[11] correlate with high metastatic potential of melanoma cells,[12−14] and endorse the tumorigenic potential of colon cancer.[9] It has also been shown that cancer cells rich in LDs tend to be more resistant to cancer therapy.[15] Thus, nowadays LDs are becoming one of the main indicators of cancer aggressiveness.[4]

Intriguingly, increase in uptake and accumulation of lipids in cancer cells is rarely described to be followed by higher expression of enzymes that can degrade TG. Quite the contrary, a lack

Received: October 31, 2017
Published: February 19, 2018

DOI: 10.1021/acs.jproteome.7b00782
J. Proteome Res. 2018, 17, 1415−1425

of adipose triglyceride lipase (ATGL) can play a role in cancer initiation.[16] The strongest phenotype in support of this finding was observed in lungs, where a loss of ATGL causes the spontaneous development of neoplasia, as shown in the model of ATGL−/− heart-rescue mice.[16] The same authors also reported that ATGL is down-regulated in various different tumor types.[16]

Because a lack of ATGL works in favor of LD formation,[17] it is possible that the reduction in the expression of this lipase is one of the initial events in malignant transformation and that its loss may render cancer cells more-aggressive. To investigate the role of ATGL in cancer cells, particularly in lungs, we selectively knocked out ATGL in the lung carcinoma cell line A549 using CRISPR/Cas9 and investigated its phenotype by fluorescence microscopy, lipidomics, proteomics, qPCR, and biochemical and cellular assays. We observed that lack of ATGL was correlated with accumulation of LDs, TG, and bioactive lipids, such as lysophospholipids and etherlipids, and an increase in proto-oncogene SRC kinase expression and activity. Moreover, ATGL knock out cells (ATGL-KO) migrated faster compared to control cells, which was dependent on SRC kinase activity. We conclude that loss of ATGL may contribute to cancer aggressiveness, and the expression level of ATGL could act as a marker for prognosis.

EXPERIMENTAL SECTION

Reagents

If not stated otherwise, chemicals were obtained from Sigma-Aldrich.

Cell Culture

A549 lung adenocarcinoma cells were obtained from CLS (Eppelheim, Germany) and cultured under standard conditions at 37 °C and 5% CO_2, in Ham's F-12K (Kaighn's) (F12K) medium supplemented with 2 g/L sodium bicarbonate, 10% fetal bovine serum (FBS), 1% penicillin/streptomycin (P/S), and 2 g/L glucose. LLC1/LL2 cells were purchased from ATCC and cultured in Dulbecco's modified Eagle's medium (DMEM) containing 10% FBS and 1% P/S.

ATGL Knockout with CRISPR-Cas9

A total of 24 h prior to transfection with CRISPR-Cas9, 100 000 A549 cells were seeded in a 6-well plate. Growth medium was exchanged for serum-free F12K medium without antibiotics. The transfection of CRISPR plasmids was performed using Lipofectamine3000 (Thermo Scientific) according to the manufacturer's protocol. ATGL CRISPR-Cas9 KO plasmid for the knockout of human ATGL was obtained from Santa Cruz (sc-401711). For the site-specific repair of the Cas9-induced double strand break a homology directed repair (HDR) plasmid (sc-401711-HDR) was co-transfected with the Cas9-plasmid. The HDR plasmid contained the red fluorescent protein (RFP) used for later evaluation of the transfection and fluorescence-activated cell sorting (FACS). A total of 1.25 μg of each plasmid per well was used during the transfection. A total of 4 hours post-transfection, 1 volume (1.5 mL) of F12K medium containing 20% FBS was added. Cells were then expanded, and single RFP-positive cells were sorted in separate wells of a 96-well plate using FACS. Single cell clones were expanded and checked for ATGL protein expression by Western blot and mRNA levels of ATGL using qPCR. As a control, A549 cells were transfected with a control plasmid from Santa Cruz (sc-418922) as stated above. Cells were then subjected to serial dilution to obtain single cell clones. Single cell clones were expanded and checked for ATGL protein expression and mRNA levels of ATGL. Furthermore, the genomic DNA of all clones (ATGL-KO and control) was extracted, and the region of the ATGL gene, where the double-strand break was induced by Cas9, was amplified by PCR and subjected to DNA sequencing (LGC Genomics, Berlin, Germany). Sequences and primers used for PCR and sequencing are shown in the supplement.

LD Imaging and Volume Analysis

A549 ATGL-KO cells and control cells were seeded on KOH-treated coverslips 24 h prior to staining. HCS LipidTOX Deep Red Neutral Lipid Stain (Thermo Fisher Scientific) and BODIPY 493/503 (Thermo Fisher Scientific) were used as lipid droplet stains. Cells were incubated with a 1:1000 dilution of boron-dipyrromethene (BODIPY) for 10 min at 37 °C and fixed for 10 min with 3.7% formaldehyde in PBS. For LipidTOX Deep Red staining, cells were first fixed with 3.7% formaldehyde in PBS for 10 min at room temperature, rinsed three times with PBS, and then stained with a 1:750 dilution of LipidTOX Deep Red. In the case of BODIPY, another two washing steps with PBS were performed prior to mounting with VECTASHIELD antifade mounting medium containing DAPI (Szabo-Scandic). Images were acquired using a Zeiss LSM 100 and a Nikon A1+ confocal laser scanning microscope with a 405 nm diode laser and 450/50 BP filter for DAPI, a 488 nm argon laser with a 525/50 BP filter for BODIPY, and a 642 nm NeHe laser and 700/75 BP filter for LipidTOX Deep Red. The analysis was performed with the FIJI (version 1.51h). For each image, a region of interest (ROI) was defined to exclude cells clipped on the edges of the images. A maximum intensity projection and application of auto-threshold using the Kapur-Sahoo-Wong (maximum entropy) method was performed prior to LD volume quantification. Based on a nucleus count, the LD volume per cell for each ROI was calculated and averaged from 55 to 86 cells derived from each of three individual knock out clones (in a total of 198 cells) and three control cell clones (in a total of 228 cells), respectively.

Targeted Lipidomics

A total of 2×10^6 A549 ATGL-KO (derived from three individual clones) and control cells were serum starved for 1 h, washed once with PBS, and harvested by scraping in PBS. Nonpolar metabolite extraction and measurement was performed as previously described.[18,19] Briefly, cell pellets were resuspended in 1 mL of PBS and added to a chloroform:methanol mixture (2:1), together with internal standards (dodecylglycerol for positive and pentadecanoic acid for negative mode). Phases were separated by centrifugation, and the chloroform phase containing the lipids was dried under stream of nitrogen. Dried lipids were resuspended in 120 μL of chloroform, and 10 μL of each sample was used for liquid chromatography−tandem mass spectrometry (LC−MS/MS) analysis based on multiple-reaction monitoring (MRM).[19] Lipid metabolites were separated on a Luna reverse-phase C5 column (50 mm × 4.6 mm, 5 μm, Phenomenex). Mobile phase A was 95:5 water/methanol, while B was 60:35:5 isopropanol/methanol/water. For the positive mode, 0.1% formic acid and 5 mM ammonium formate were added to both A and B; for the negative mode, solvents were supplemented with 0.1% ammonium hydroxide. The flow rate was 0.5 mL/min. Agilent 6430 QQQ was used for MS analysis with following parameters: capillary voltage, 3.0 kV; fragmentor voltage, 100 V; drying gas temperature, 350 °C; drying gas flow, 10 L/min, and nebulizer gas pressure, 35 psi. Different collision energies were used for each SRM transition according to previous optimization.

DOI: 10.1021/acs.jproteome.7b00782
J. Proteome Res. 2018, 17, 1415−1425

Relative abundance of each monitored metabolite was obtained by integrating the area under the peak for selected transition, normalized on the area of the internal standard from the corresponding run. To correct for slight differences in amounts of injected samples, the obtained relative abundance of each metabolite was further normalized on the area of the total ion chromatogram of the corresponding sample, which represents the sum of all monitored transitions. The normalized result list was imported to Perseus (version 1.5.8.5),[20] in which the cutoff criteria for significance upon multiple-testing correction was: unpaired Student t test p-value of <0.05, a permutation-based false discovery rate (FDR) of <0.05, and an S_0 value of 1.5.

Proteomics

Cell pellets from 4 ATGL-KO and 4 control A549 cell clones were collected after trypsinization, washed 3 times with PBS, and lysed by sonication in lysis buffer (100 mM Tris, pH = 8, 1% sodium dodecyl sulfate (SDS), 10 mM tris(2-carboxyethyl)-phosphine hydrochloride (TCEP), 40 mM 2-chloroacetamide). A total of 200 μg of protein per sample was further processed and digested according to a modified FASP protocol.[21] LC−MS/MS was performed by nano-LC on an Acclaim PepMap RSLC C18 nanocolumn (2 μm, 50 × 75 μm) (Thermo Scientific) coupled to a maXis II ETD Q-TOF (Bruker Daltonics, Germany) run in positive mode.

For label-free quantitative proteomics data and statistical analysis, MaxQuant (version 1.5.8.3)[22] and Perseus (version 1.5.8.5)[20] were employed, respectively. MaxQuant parameters included the match between run feature in a retention time window of 1 min and an alignment window of 20 min. For the database search, a FDR of 1% was allowed.

Statistical analysis in Perseus was performed after filtering the data set under the criteria that all four values in at least one group must be valid (greater than zero), with the consequent imputing of missing values from normal distribution with regards to the total data matrix. Following steps included two-sided unpaired t test with a S_0 value of 2 and permutation-based FDR control at a level of 1%.

Principle component analysis (PCA) was carried out on the preprocessed data set with centered variables and hierarchical clustering (HC) employing Euclidean distance measure and Ward's agglomeration method.[23] For these purposes, the R statistical computing software (v. 3.2.2, https://www.r-project.org/) was used. PCA was performed with the function "prcomp", while for HC, the functions "dist" and "hclust" as well as the function heatmap.2 in R gplots (v. 3.0.1) were employed (https://CRAN.R-project.org/package=gplots).

For functional analysis of proteomic data, enrichment of gene ontology (GO) terms of biological processes of proteins with a minimum absolute difference of log2 label-free quantitation (LFQ) intensities between groups of 0.5 was performed as described in detail in the Supporting Information. The mass spectrometry proteomics data was deposited to the ProteomeXchange Consortium[24] (http://proteomecentral.proteomexchange.org) via the PRIDE partner repository with the data set identifier PXD007223.

MS-Based Validation of Differential SRC Protein Abundance

Samples were prepared as described in the Proteomics section. In addition, the same LC setup was used but coupled to an Orbitrap Velos Pro as detector (Thermo Scientific), operated as well in positive mode with dynamic exclusion enabled. A parent mass list of expected SRC peptides was introduced as an inclusion list (masses: 443.73, 446.76, 494.26, 516.77, 520.30, 608.30, 642.83, 736.05, and 856.92). Data were analyzed with MaxQuant as described above.

qPCR

Total RNA was isolated from cells using the RNA easy kit (Qiagene, Netherlands). qPCR was performed according to the manufacturer's instructions with Maxima SYBR Green (Thermo Fisher Scientific, USA). Corresponding cDNA was synthesized either with Maxima RT (Thermo Fisher Scientific, USA) or QuantiTect Reverse Transcription Kit (Qiagen, Netherlands). Cyclophilin A was used as housekeeping gene with the primers 5′-CCCACCGTGTTCTTCGACATT-3′ (forward) and 5′-GGACCCGTATGCTTTAGGATGA-3′ (reverse). The primers for SRC were 5′-TGTTCGGAGGCTTCAACTCC-3′ (forward) and 5′-TGTGTTGTTGACAATCTGGAGC-3′ (reverse). For ATGL, two sets of primers were used: (1) forward 5′-GCTTC CTCGGCGTCTACTAC-3′ and reverse 5′-CAATGAA CTTGGCACCAGCC-3′ and (2) 5′- GGCTTCCTCGGCGTC TACTA-3′ (forward) and 5′-TTTACCAGGTTGAAG-GAGGGG-3′ (reverse).

Lentiviral ATGL Knock-in

Lentiviral constructs for human ATGL (pLV[Exp]-Neo-EFS > hPNPLA2[ORF016935]) and control green fluorescent protein (GFP) vector (pLV[Exp]-Neo-EFS > EGFP) were acquired from VectorBuilder (Cyagen Bioscience). IDs for ATGL vector VB17120-1187tqx and for GFP vector VB171206-1221hfs can be used to access detail vector information on www.vectorbuilder.com. Third-generation packaging system needed to support the formation of viral particles was obtained from Addgene and consisted of pMD2.G (Addgene plasmid no. 12259), pRSV-Rev (Addgene plasmid no. 12253), and pMDLg/pRRE (Addgene plasmid no. 12251). HEK293 cells were obtained from CLS (Eppelheim, Germany).

The day before transfection (day 0), HEK293 cells were seeded in 10 cm dishes in triplicates for each of the two constructs (ATGL and GFP). The next day (day 1), medium from HEK293 was exchanged for 6 mL of DMEM containing 10% heat-inactivated serum (HIS). For every transfection, 600 μL of serum-free DMEM was combined with 24 μL of Lipofectamine LTX (Thermo Scientific) in a 1.5 mL Eppendorf tube and incubated for 5 min. In another tube, 600 μL of DMEM was mixed with 2 μg of each packaging plasmid and 2 μg of ATGL or GFP vector. The contents of both tubes were combined and incubated for 30 min before their addition to HEK293 cells and overnight incubation. On the following day, the medium from the HEK293 cells was replaced with fresh DMEM/HIS medium, and the target cells (three individual ATGL-KO A549 clones) were seeded to reach 50% confluency. On day 4, the medium of the target cells was replaced with 5 mL of full DMEM containing 10 μg/mL polybrene. Viral soup from the HEK293 cells was aspirated using a 10 mL syringe and filtered onto the target cells through a 0.45 μm filter. Same procedure was repeated the following day (day 5). Target cells were incubated for 24 h, after which the medium was replaced (day 6). On day 7, the medium was changed to 10 mL of full RPMI containing 1000 μg/mL gentamicin. Antibiotic containing medium was refreshed every 2−3 days, and the cells were kept in culture for 2 weeks prior to Western blot analysis and migration assay.

Western Blotting

Cells were harvested either in 100 mM TrisHCl pH 8 or CST buffer (Cell Signaling Technology (CST, Danvers, MA). For atglistatin treatment, cells were incubated with 80 μM atglistatin

DOI: 10.1021/acs.jproteome.7b00782
J. Proteome Res. 2018, 17, 1415−1425

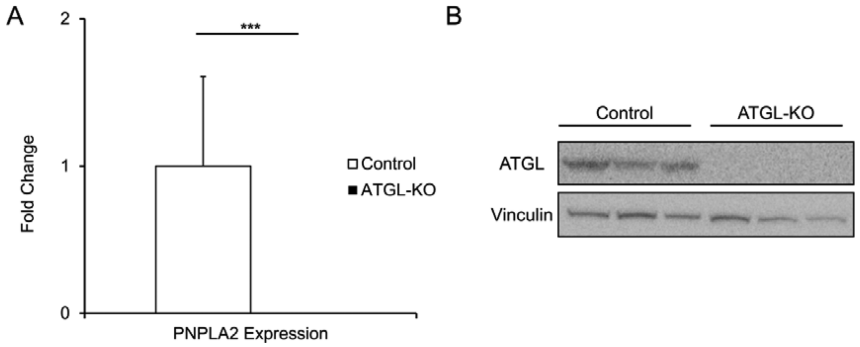

Figure 1. CRISP-R/Cas9 ATGL-KO leading to the loss of ATGL gene and protein expression in A549 cells. (A) qPCR of patatin like phospholipase domain containing 2 (PNPLA2, ATGL gene), $N = 3$ cell lines derived from single cell clones per group, data from two individual experiments, where triple asterisks indicate $p < 0.001$. Cyclophilin A was used as house-keeping gene. (B) Western blot of ATGL protein. Shown is one of three comparable experiments.

(a kind gift from Prof. Rudolf Zechner, University of Graz) or DMSO (control) for 16 h prior to harvesting. Antibodies against ATGL (no. 2138S), SRC (no. 2109), and phospho-SRC (pSRC, no. 6943) were purchased from CST. Vinculin or β-actin was used as a loading control (antibodies were obtained from CST (no. 4650) and Sigma-Aldrich (no. A5441), respectively). HRP-linked antirabbit antibody from CST (no. 7074) was employed as secondary antibody except for the detection of β-actin, in which an antimouse secondary antibody linked to HRP was used (no. 7076). Proteins from 20 to 30 μg cell lysates were separated on a precast SDS-polyacrylamide gel electrophoresis (SDS-PAGE) gel (Invitrogen). Proteins were then blotted onto a PVDF membrane (Bio-Rad). Free binding sites on the membranes were blocked with either 5% BSA in Tris-buffered saline containing Tween 20 (TBS-T) (pSRC and SRC) or 5% skim milk in TBS-T (ATGL, β-actin, and vinculin). Primary antibodies were diluted in corresponding blocking buffers and incubated with membranes overnight at 4 °C. Membranes were washed thrice for 10 min in TBS-T and then incubated with secondary antibody for 1 h at room temperature. Antibody bound proteins were visualized after incubation with ECL (GE Healthcare) and detected on a ChemiDoc System (Bio-Rad).

Migration

Gap Closure ("Scratch") Assay. A total of 2×10^5 cells were seeded per well of a 12-well plate in triplicates. Upon reaching confluency, cells were washed with PBS and supplemented with fresh medium containing either 20 nM of SRC inhibitor KX2−391 (Selleckchem, Germany) or DMSO vehicle. Pictures were taken using an inverted microscope at 4× magnification. Gap size was measured at three different points using ImageJ software (version 1.46r).

Transwell Assay. Cells ($N = 3$ per cell line or condition) were serum-starved for 1 h prior to the assay. A total of $5-10 \times 10^4$ cells were seeded on top of the transwell chambers in serum free medium. For the migration experiment with SRC inhibitor, medium contained either 20 nM of KX2−391 or DMSO vehicle, whereas for atglistatin treatment, 80 μM atglistatin or DMSO vehicle was added to the medium. The bottom of the transwell chamber was precoated with collagen, and cells were allowed to migrate through the membrane during 20−48 h, after which they were stained, fixed and visualized (Diff Quick Stain kit, Thermo Fisher). In the case of LLC1/LL2 cells the upper part of the transwell chamber was coated with collagen to facilitate cell spreading, and cells were allowed to migrate to the lower chamber containing 10% FBS medium. A total of three fields per well at 20× magnification were used to count the cells.

Statistics

If not stated otherwise, a two-sided unpaired t test was performed with $p < 0.05$ as significance threshold. The mean and standard error of mean are depicted in bar plots.

RESULTS

ATGL Loss and Lipid-Droplet Accumulation in A549 Lung Carcinoma Cells

CRISPR-Cas9 methodology introduces a double-strand break (DBS), which, naturally, would be repaired by the process of nonhomologous end joining (NHEJ), a preferential DBS repair mechanism.[25] Considering the error-prone nature of NHEJ,[26] we introduced an HDR plasmid, which facilitated knockout clone selection and validation, allowing us to sequence the area around the expected DBS with primers targeting the sequence of the HDR plasmid. Sequencing of the ATGL-KO clones revealed that Cas9 induced the double-strand break in exon 3 of the ATGL gene and deletion of the ATGL ORF between bp 2868 and 3604 due to the integration of the HDR plasmid (Tables S1A-C). This resulted in the absence of ATGL mRNA (Figure 1A) and protein (Figure 1B) in the isolated single cell clones.

Because ATGL is a major TG lipase, its loss caused prominent LD accumulation in A549 ATGL-KO cells (Figure 2A). The LD volume, as determined in about 200 ATGL-KO cells derived from three single cell clones and, similarly, in control cells, was found to be four times higher than in control cells (Figure 2B).

ATGL-KO Lung Cancer Cells and Accumulation of Triacylglycerols and Bioactive Lipids

The accumulation of TG, the substrate of ATGL and a major component of LDs, in ATGL-KO cells was confirmed by lipidomics. Out of about 180 quantified lipid species (Table S2) from targeted measurements, TGs were found to be most prominently enriched in ATGL-KO.

Next to TG, several phospholipids and sphingolipids, as well as palmitoyl carnitine were also found to be more abundant in ATGL-KO cells. Furthermore, we observed an upregulation of lysophospholipids, particularly lysophosphatidylcholines (LPC), which are known to have signaling function.[27−29] In addition, we detected higher levels of several ether lipids, members of another class of bioactive lipids[30] in ATGL-KO cells (Figure 3).

ATGL Loss and Up-regulation of SRC Kinase in A549 Lung Carcinoma Cells

To reveal whether the observed lipid changes in ATGL-KO were accompanied by adaptations of the proteome, label-free quantitative

DOI: 10.1021/acs.jproteome.7b00782
J. Proteome Res. 2018, 17, 1415−1425

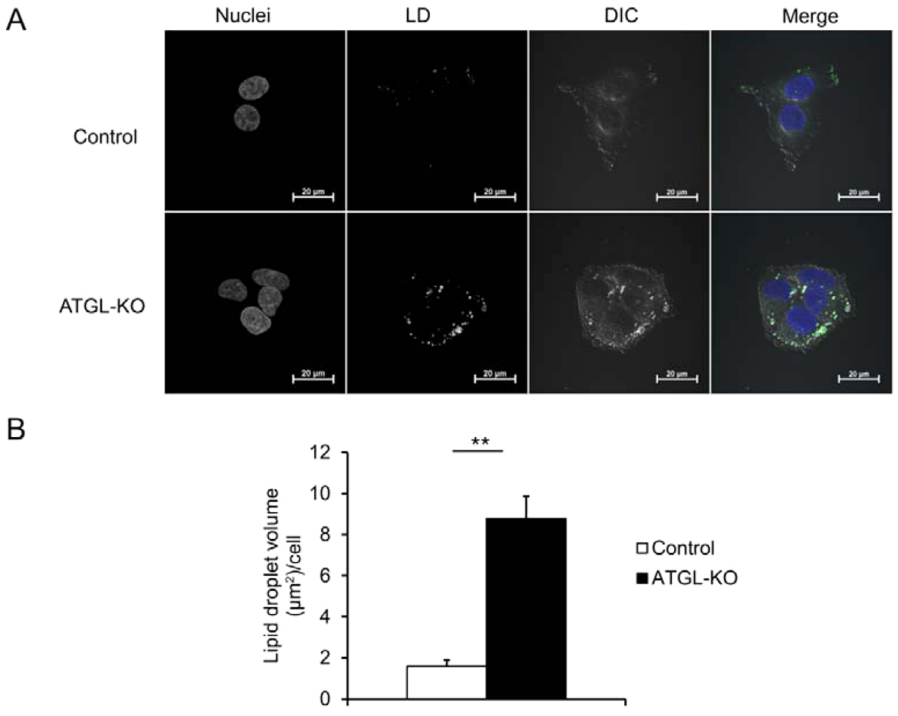

Figure 2. Loss of ATGL induces LD accumulation in ATGL-KO cells. (A) Fluorescence microscopy of cells labeled with DAPI for cell nuclei and BODIPY for LD visualization. (B) Quantitative analysis of LD content (N = 3 cell lines derived from single cell clones per group, >50 individual cells per cell line); double asterisks indicate $p < 0.01$.

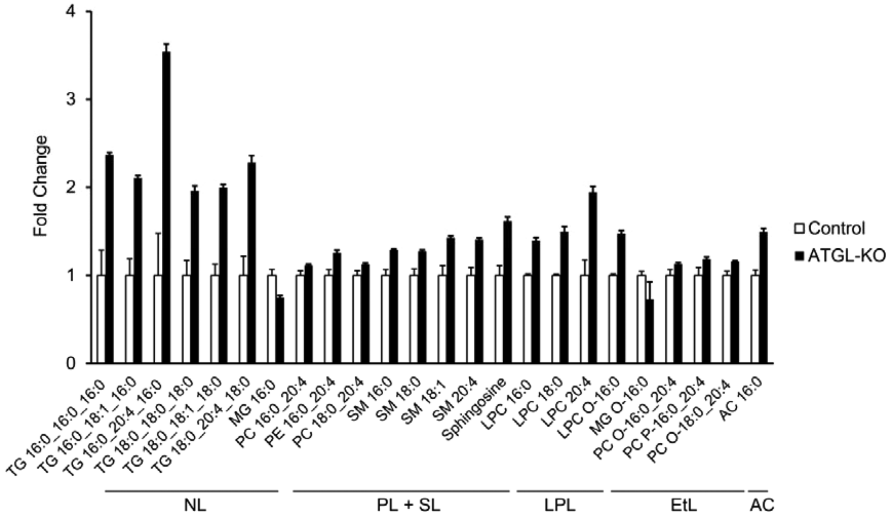

Figure 3. Altered lipid metabolites in A549 ATGL-KO cells. Reported is fold change as compared to control. N = 3 ATGL-KO cell lines derived from single cell clones, N = 5 replicates per cell line, Welch t test $p < 0.05$, multitest correction: permutation-based FDR < 0.05, S0 = 1.5 (NL, neutral lipids; PL + SL, phospholipids and sphingolipids; LPL, lysophospholipids; EtL, ether lipids; AC, acylcarnitine; TG, triacylglycerol; MG, monoacylglycerol; PC, phosphatidylcholine; PE, phosphatidylethanolamine; SM, sphingomyelin and LPC, lysophosphatidylcholine).

proteomics screening was performed (Figure 4) using the LFQMax algorithm.[31] LC−MS/MS proteomics measurements (N = 4 biological replicates per group) yielded approximately 2100 quantified proteins per single run. Principal component analysis (Figure 4B) and hierarchical clustering (Figure 4C, Figure S1) clearly discriminated ATGL-KO from control cells.

LFQ output results usually contain some missing values due to the stochastic nature of the data-dependent acquisition of fragmentation spectra in mass spectrometry thus making imputation a necessary step to achieve meaningful statistical analysis. To constrain the imputation algorithm as much as possible, we filtered the data matrix to only keep those proteins that had reported values in all 4 samples of at least 1 group (679 proteins). After consequent stringent statistical analysis involving correction for multiple-testing by permutation-based FDR, two proteins were found to be changed between the groups (Figure 4A and Table S3). The proto-oncogene kinase SRC[32] was the most significantly up-regulated protein in ATGL-KO cells. Being involved in various biological processes, SRC greatly contributed to the biological processes observed in the GO term enrichment analysis in the set of proteins with a minimum absolute difference of 0.5 of the log2 LFQ intensities in the KO versus WT group (Figure 4D and Table S4), such as innate immune response-activating signal transduction, stimulatory C-type lectin receptor signaling pathway

DOI: 10.1021/acs.jproteome.7b00782
J. Proteome Res. 2018, 17, 1415−1425

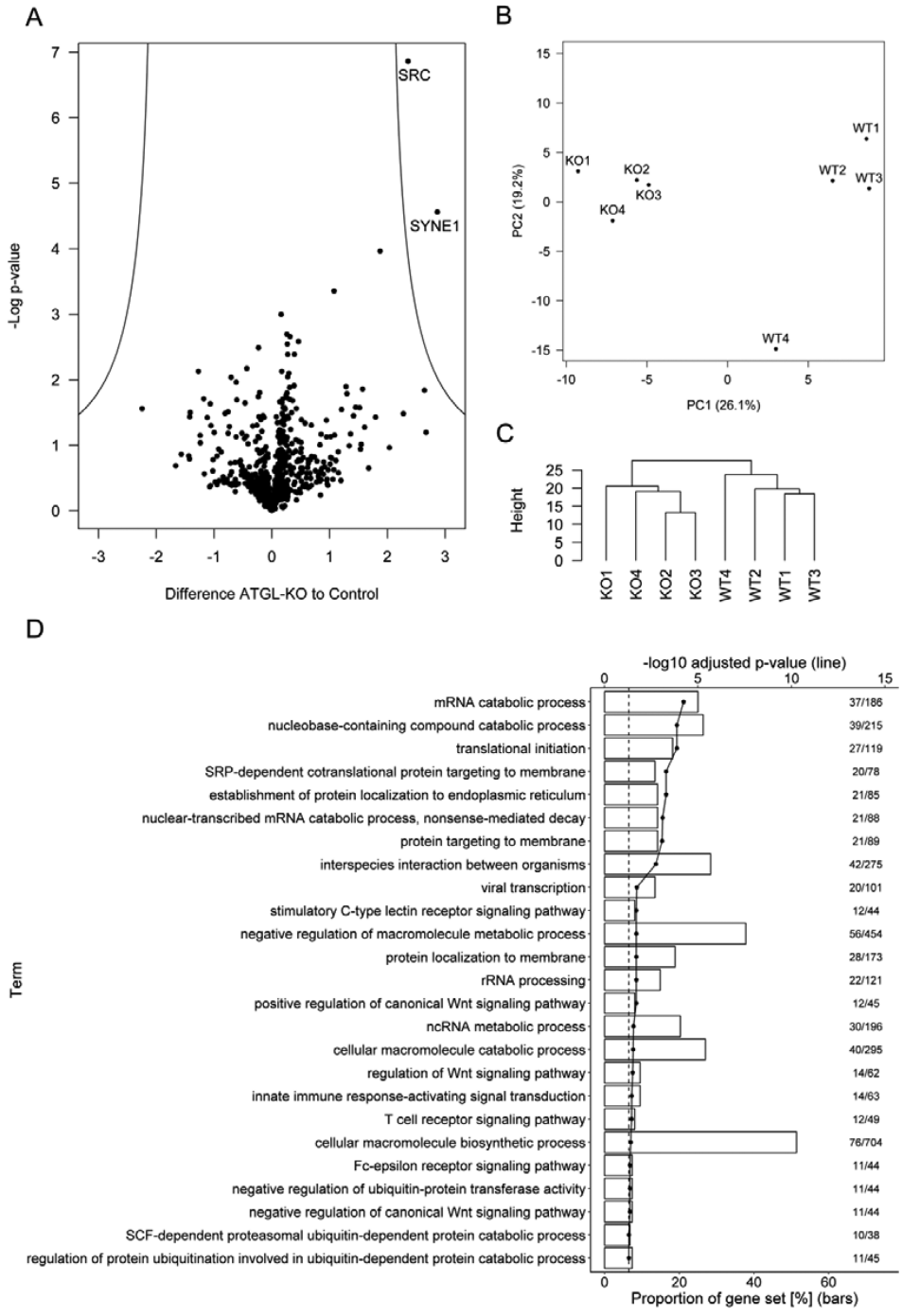

Figure 4. Label-free quantitation (LFQ) of ATGL-KO cells proteome reveals two proteins and significant up-regulation in ATGL-KO cells ($N = 4$ cell lines derived from single cell clones per group). (A) Volcano plot of LFQ data (−log p-values (*t* test) plotted vs differences of log2 LFQ intensities; cut-off *p*-value of <0.05; multitest correction: permutation-based FDR of < 0.01; S0 = 2). (B) PCA of LFQ data sets of ATGL-KO vs control (wildtype (WT)). (C) Dendrogram obtained by hierarchical clustering of LFQ data sets. (D) Over-represented gene ontology (GO) terms of biological processes in the set of proteins with a minimum absolute difference of 0.5 of the log2 LFQ intensities in the KO vs the WT group. The dotted line shows the FDR adjusted *p*-value (−log10(*p*-value), axis at the top) for over-represented terms, and the dashed line indicates the significance threshold of 0.05. The length of the bars represents the proportion of the protein set of interest (Entrez IDs of the corresponding genes) that is mapped to the respective term (axis at the bottom). Numbers to the right of the bars indicate the number of proteins in the protein set of interest that are mapped to the respective term, the number of proteins shared by the term, and the background protein set (term size).

and positive regulation of canonical Wnt signaling pathway. Next to signaling, mainly processes related to protein translation and degradation were found to be enriched.

To validate our finding that SRC protein is elevated in A549 ATGL-KO cells, we carried out a semitargeted mass spectrometry based SRC protein measurement, which was in line with the LFQ results (Figure 5A). To assess whether the active phosphorylated form of SRC was also increased, Western blotting of phospho-SRC Y416 (pSRC) and total SRC protein was performed revealing 2- to 3-fold higher levels of SRC and pSRC in ATGL-KO cells (Figure 5C,D). In addition, the increased expression of the SRC gene in ATGL-KO was also observed on mRNA level by

DOI: 10.1021/acs.jproteome.7b00782
J. Proteome Res. 2018, 17, 1415−1425

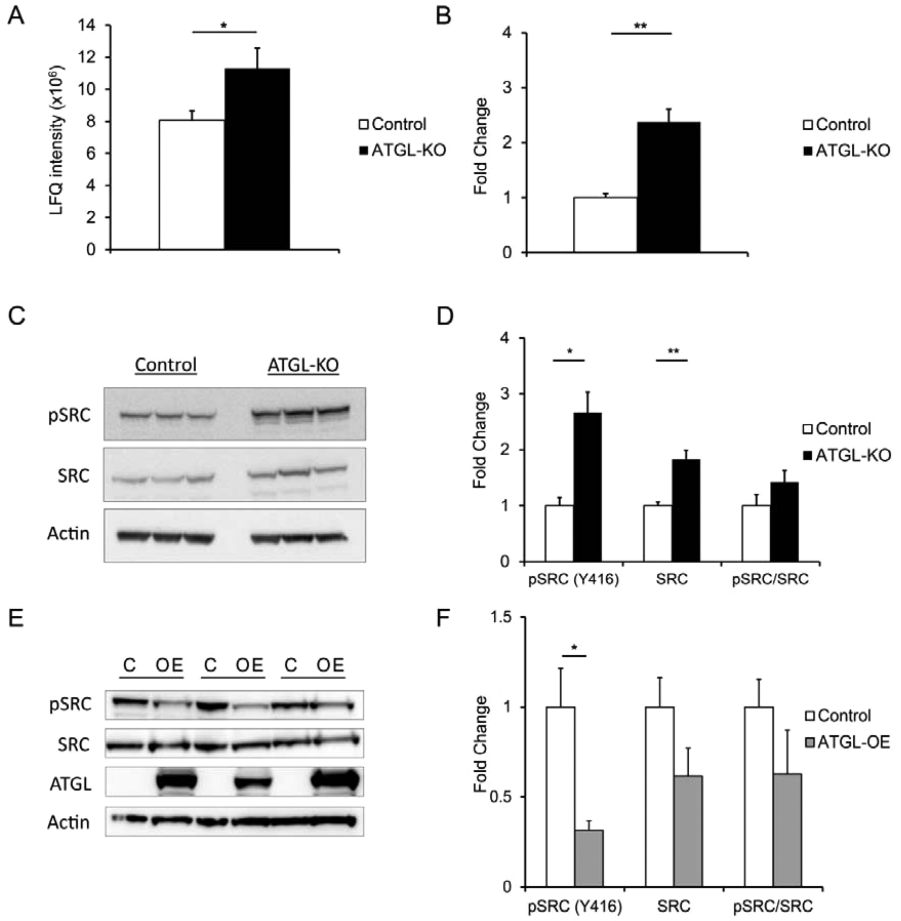

Figure 5. SRC up-regulation on the mRNA, protein, and phosphoprotein levels in ATGL-KO and its reversal by stable re(over)expression of ATGL. (A) LFQ values for SRC protein from semitargeted LC−MS/MS measurement (N = 4−5 cell lines derived from single cell clones per group). (B) SRC mRNA levels (N = 3 cell lines derived from single cell clones per group). (C) Western blot for SRC and pSRC (Y416); actin as loading control. (D) Volume analysis of C. (E) Western blot for pSRC, SRC, and ATGL upon ATGL over-expression in three single-cell-derived ATGL-KO A549 clones (with actin as loading control). (F) Volume analysis of E; single asterisks indicate a p-value of <0.05, and double asterisks indicate a p-value of <0.01.

qPCR (Figure 5B). To investigate whether reintroducing ATGL could reverse increased SRC protein expression and phosphorylation in the ATGL-KO, we lentivirally over-expressed ATGL in three single-cell-derived ATGL-KO clones of A549 cells. This resulted in prominent ATGL expression, which clearly reversed activation of SRC (Figure 5E,F).

Increased Migration of ATGL-KO A549 Lung Carcinoma Cells and Dependency on SRC Kinase Activity and Reversibility

To address potential changes in aggressiveness of lung cancer cells lacking ATGL, growth curves and migration assays were performed. Growth was found to be similar to slightly enhanced by the deletion of ATGL (Figure S2). However, both transwell and wound healing (scratch) assay demonstrated that ATGL-KO cells were able to migrate faster (Figure 6A,B). The phenotype was observed in both serum-free conditions when cells were chemo-attracted to collagen (by transwell assay, Figure 6A) as well as in serum-rich condition (by scratch assay, Figure 6B).

Interestingly, both hits from the proteomics screen were shown to be involved in cellular migration.[33,34] We thus performed a follow-up experiment to investigate the role of SRC in controlling cell migration in A549 cells depleted of ATGL. For this purpose, migration assays were performed in the presence of a highly selective SRC inhibitor[35] (Figure 6A,B). The inhibition of SRC reduced the number of ATGL-KO cells that migrated through the pores of the transwell chamber without influencing the migration of control cells (Figure 6A). The used concentration did not affect the cell survival of ATGL-KO or control cells (Figure S3). A similar result was obtained by scratch assay (Figure 6B).

Moreover, re(over)expression of ATGL in ATGL-KO A549 clones reversed the observed phenotype. It reduced the amount of LDs (Figure S4AB) and activation of SRC (Figure 4EF), consequently decreasing the migratory potential of the ATGL-KO cells (Figure S4CD).

Pharmacological Inhibition of ATGL and SRC Activation and Increase of Migratory Potential in Murine LLC1/LL2 Lewis Lung Carcinoma Cells and AML12 Hepatocytes

With the purpose of further verifying the connection between impaired lipolysis and pro-oncogenic signaling, we pharmaceutically inhibited ATGL in murine LLC1/LL2 Lewis lung carcinoma cells using atglistatin,[36] an inhibitor of murine ATGL. After 16 h of treatment with 80 μM atglistatin, the activation of SRC could be detected by elevated pSRC (Figure 7A,B). While the treatment did not induce the expression of SRC protein in the given time frame, the effect was prominent enough to boost the migratory potential of the cells (Figure 7C,D). A similar

DOI: 10.1021/acs.jproteome.7b00782
J. Proteome Res. 2018, 17, 1415−1425

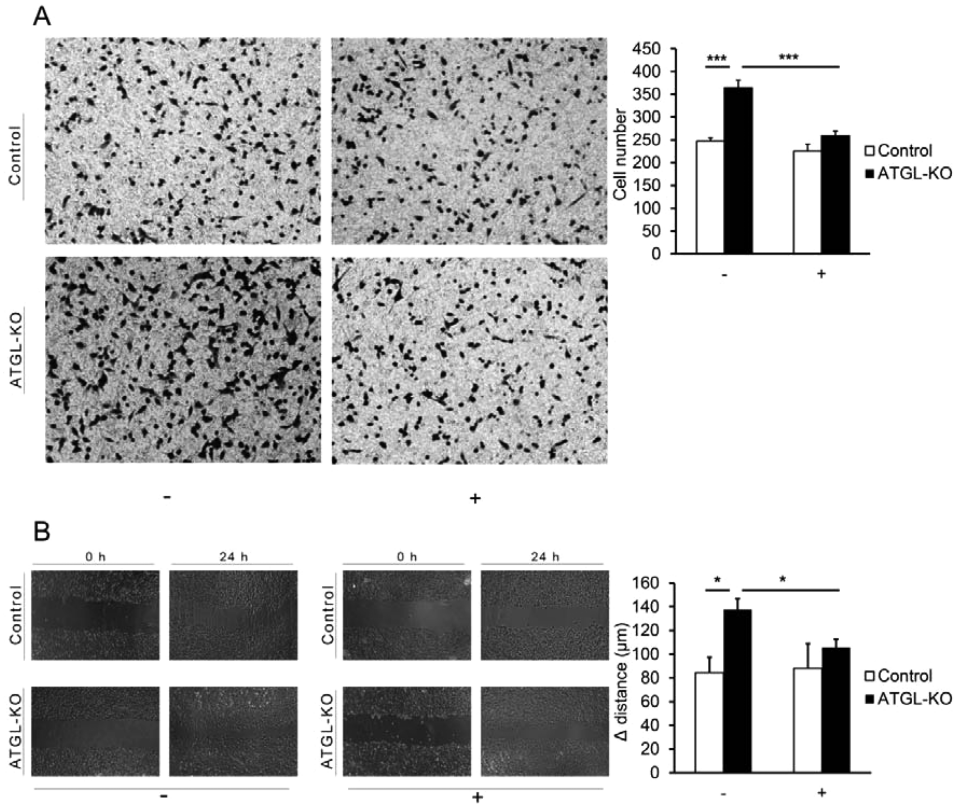

Figure 6. Faster migration of ATGL-KO cells and SRC dependency. A549 ATGL-KO and control cells were treated with either 20 nM of KX2−391 (+) or vehicle (DMSO) (−) (A) Representative transwell assay and numbers of migrated cells in the transwell assay. (B) Representative scratch assay and the covered distance (resembling gap closure) in panel B. $N = 3$ ATGL-KO cell lines derived from single cell clones, $N = 3$ replicates per cell line; double asterisks indicate a p-value of <0.01, and triple asterisks indicate a p-value of <0.001.

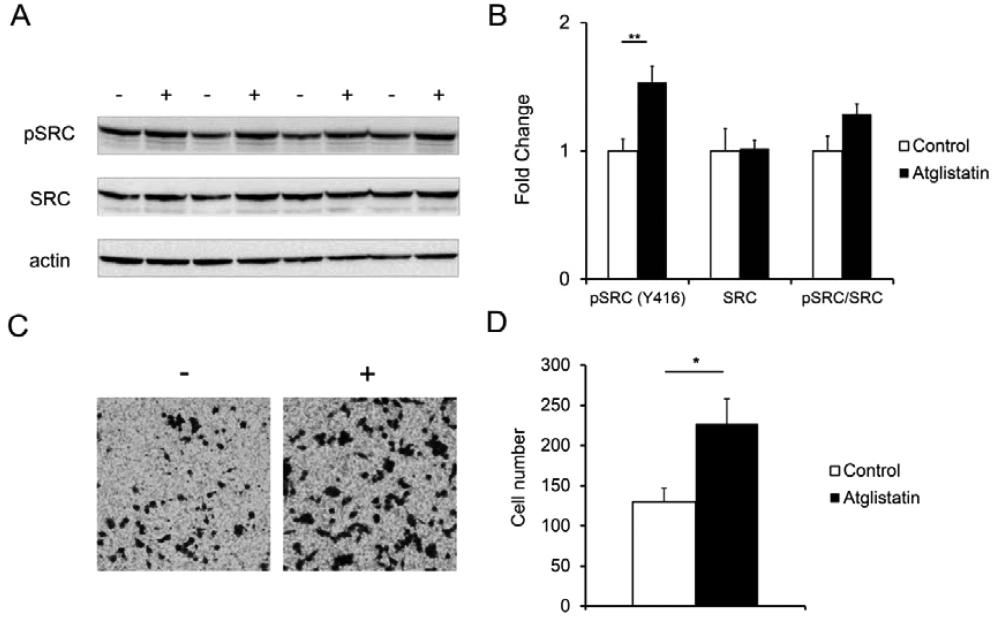

Figure 7. Pharmacological inhibition of ATGL in murine LLC1/LL2 Lewis lung cancer cells, activation of SRC, and increase in their migratory potential. (A) Western blot of LLC1/LL2 cells for pSRC (Y416), SRC and β-actin (loading control). (B) Corresponding volume analysis. (C) Transwell migration assay, in which a dash indicates the control (DMSO vehicle) and a plus sign indicates atglistatin treatment (80 μM). (D) Number of migrated cells in panel C. $N = 3$ per condition; a single asterisk indicates a p-value of <0.05, and double asterisks indicate a p-value of <0.01.

phenotype was observed in another murine cell line, namely AML12 mouse hepatocytes (Figure S5). This was a particularly interesting finding because AML12 cells are not tumorigenic, and yet ATGL inhibition rendered them more aggressive in culture.

DISCUSSION

Changes in lipid metabolism can have a prominent effect on cancer phenotype.[4] However, reports regarding the role of lipases in cancer are scarce. ATGL has been found to be down-regulated in

DOI: 10.1021/acs.jproteome.7b00782
J. Proteome Res. 2018, 17, 1415−1425

several different cancer types.[16] In contrast, the enzyme responsible for monoacylglycerol hydrolysis, monoacylglycerol lipase (MGL), is highly expressed in aggressive human cancer cells and primary tumors, where it regulates a fatty-acid network enriched in oncogenic signaling lipids that promotes migration, invasion, survival, and *in vivo* tumor growth.[37] Impairments in MGL-dependent tumor growth are rescued by a high-fat diet, indicating that exogenous sources of fatty acids can contribute to malignancy in cancers lacking MGL activity. The contribution of external lipids to aggressive cancer phenotype is also reported in breast cancer,[38] providing yet another link between obesity, a high-fat diet, and cancer incidence. In line with these findings, it was recently discovered that high levels of the fatty acid receptor CD36 and palmitic acid or a high-fat diet are associated with initiation of metastasis in human oral cancer.[39] The authors also observed concomitant higher expression of beta-oxidation genes to avoid lipotoxicity.

Accordingly, we show that the depletion of ATGL leads to LD accumulation associated with a more-aggressive cancer phenotype, including higher levels of pro-oncogenic signaling lipids such as lysophosphatidylcholines (LPCs) and ether lipids, activation of pro-oncogenic SRC kinase signaling, and increased migration. While it was reported before that ATGL knock-down slows growth of A549 lung cancer cells,[40] we did not observe a significant effect on growth in the complete knock out. The same authors also observed reduced migration of A549 lung cancer cells upon treatment with atglistatin, an inhibitor for murine but not human ATGL,[36] which has thus to be attributed to off target effects. In contrast, we observe an opposite effect when we use atglistatin in murine cell lines, in which the inhibition of ATGL leads to activation of SRC and increased migratory potential in both LLC1/LL2 cells and AML12 hepatocytes.

The reintroduction of ATGL in ATGL-KO A549 cells by stable lentiviral over-expression reduced the size and number of LDs and decreased the activation of SRC, confirming the link between ATGL activity, LD accumulation, and SRC signaling. SRC kinase is commonly up-regulated in cancer and can support migration potential and tumor progression.[41] From the combined data, we conclude that cancer cells do not necessarily rely on intracellular lipolysis and are, over time, able to rewire their metabolism accordingly. However, this may result in a higher dependence on exogenous nutrients to sustain tumor growth potentially leading to higher aggressiveness and metastasis, as the cancer cells are driven to obtain the required nutrients. LD accumulation following a reduction of lipolytic activity and the increased uptake of external lipids may also act as a potent buffer to prevent lipotoxicity of free fatty acids.[42−45] Moreover, lipid accumulation in the form of LDs may provide substrates for various enzymes that can produce pro-oncogenic signaling lipids[46] or even drive the expression of other enzymes (e.g., phospholipases). Consistently, we observe an increase in lysophospolipids and ether lipids in cells lacking ATGL. This is an interesting finding as both LPCs and ether lipids are reported to be involved in inflammation, cancer initiation and progression, usually contributing to more-aggressive phenotypes.[47−52] Importantly, a positive correlation has been observed between the tumorogenicity of cells and their ether lipid content, with the cells containing the highest level of ether lipids being the most-invasive ones.[53]

LPCs can bind to different G-protein coupled receptors (GPCRs), with the highest affinity toward G2A (from G2 accumulation) GPCR.[54,55] Once bound, LPCs can modulate the activity and expression of different signaling proteins including serum-responsive element, mitogen-activated protein kinase, adenylyl cyclase, and phospholipase C.[29,50,54] Furthermore, increased levels of LPCs as observed in ATGL-KO lung cancer cells have been described to lead to SRC kinase activation.[27] Intriguingly, we could also show that inhibition of SRC kinase activity is sufficient to abolish the more aggressive cell migration and wound-healing characteristics of ATGL-KO lung cancer cells, thus mechanistically linking increased neutral lipid storage following the loss of lipase activity to cancer-cell aggressiveness.

CONCLUSIONS

We report here that the loss of ATGL in lung cancer cells leads to TG and concomitant LD accumulation, elevated levels of ether- and lysophospholipids, and a pro-invasive phenotype mediated by the activation of pro-oncogenic signaling via SRC kinase. Our findings are in line with previous observations that increased LD content is associated with a more-aggressive cancer phenotype[56,57] and that ATGL is often lost in cancer.[16] However, we establish here for the first time a mechanistic link between neutral lipid accumulation caused by ATGL loss and elevated cancer-cell aggressiveness.

ASSOCIATED CONTENT

Supporting Information

The Supporting Information is available free of charge on the ACS Publications website at DOI: 10.1021/acs.jproteome.7b00782.

A table showing the lipidomics results of A549 cell clones. (XLSX)

A table showing a proteomics result list of proteins of A549 cell clones upon filtering for four valid values per group. (XLSX)

A table showing Gene Ontology (GO) analysis of A549 cell clones. (XLSX)

Additional details on experimental methods. A table showing sequences and alignments of A549 ATGL-KO clones. Figures showing hierarchical clustering, lentiviral re(over)expression of ATGL, growth of A549 ATGL-KO clones, SRC inhibitor treatment, and the inhibition of ATGL in AML12 cells. (PDF)

AUTHOR INFORMATION

Corresponding Author

*E-mail: ruth.birner-gruenberger@medunigraz.at. Phone: +43-316-385-72962.

ORCID

Daniel K. Nomura: 0000-0003-1614-8360
Matthias Schittmayer: 0000-0003-3249-655X
Ruth Birner-Gruenberger: 0000-0003-3950-0312

Present Address

#Department of Molecular Systems Biology, Helmholtz Centre for Environmental Research, UFZ, 04318 Leipzig, Germany.

Author Contributions

T.T. and K.F. contributed equally. T.T., K.F., M.S., D.K.N., and R.B.-G devised the study, and T.T., K.F., and R.B.-G wrote the manuscript. T.T., K.F., J.G., and L.W. performed the experiments. B.P. and G.G.T. contributed to data analysis. All authors have given approval to the final version of the manuscript.

Notes

The authors declare no competing financial interest.

DOI: 10.1021/acs.jproteome.7b00782
J. Proteome Res. 2018, 17, 1415−1425

■ ACKNOWLEDGMENTS

This work was supported by Austrian Science Fund (FWF) projects nos. P26074, J-3983, and KLI425; the doctoral school "DK Metabolic and Cardiovascular Disease" (W1226); and by the Austrian Ministry of Science, Research, and Economy (HSRM project OMICS Center Graz). The authors thank Stefan Spoerk for excellent technical assistance.

■ REFERENCES

(1) Hanahan, D.; Weinberg, R. A. Hallmarks of cancer: the next generation. *Cell* **2011**, *144* (5), 646−74.
(2) Baenke, F.; Peck, B.; Miess, H.; Schulze, A. Hooked on fat: the role of lipid synthesis in cancer metabolism and tumour development. *Dis. Models & Mech.* **2013**, *6* (6), 1353−63.
(3) Zhang, F.; Du, G. Dysregulated lipid metabolism in cancer. *World J. Biol. Chem.* **2012**, *3* (8), 167−74.
(4) Beloribi-Djefaflia, S.; Vasseur, S.; Guillaumond, F. Lipid metabolic reprogramming in cancer cells. *Oncogenesis* **2016**, *5*, e189.
(5) Currie, E.; Schulze, A.; Zechner, R.; Walther, T. C.; Farese, R. V., Jr. Cellular fatty acid metabolism and cancer. *Cell Metab.* **2013**, *18* (2), 153−61.
(6) Santos, C. R.; Schulze, A. Lipid metabolism in cancer. *FEBS J.* **2012**, *279* (15), 2610−23.
(7) Thiam, A. R.; Farese, R. V., Jr.; Walther, T. C. The biophysics and cell biology of lipid droplets. *Nat. Rev. Mol. Cell Biol.* **2013**, *14* (12), 775−86.
(8) Boren, J.; Taskinen, M. R.; Olofsson, S. O.; Levin, M. Ectopic lipid storage and insulin resistance: a harmful relationship. *J. Intern. Med.* **2013**, *274* (1), 25−40.
(9) Tirinato, L.; Liberale, C.; Di Franco, S.; Candeloro, P.; Benfante, A.; La Rocca, R.; Potze, L.; Marotta, R.; Ruffilli, R.; Rajamanickam, V. P.; Malerba, M.; De Angelis, F.; Falqui, A.; Carbone, E.; Todaro, M.; Medema, J. P.; Stassi, G.; Di Fabrizio, E. Lipid droplets: a new player in colorectal cancer stem cells unveiled by spectroscopic imaging. *Stem Cells* **2015**, *33* (1), 35−44.
(10) Sanna, C.; Rosso, C.; Marietti, M.; Bugianesi, E. Non-Alcoholic Fatty Liver Disease and Extra-Hepatic Cancers. *Int. J. Mol. Sci.* **2016**, *17*, (12).71710.3390/ijms17050717
(11) Menard, J. A.; Christianson, H. C.; Kucharzewska, P.; Bourseau-Guilmain, E.; Svensson, K. J.; Lindqvist, E.; Chandran, V. I.; Kjellen, L.; Welinder, C.; Bengzon, J.; Johansson, M. C.; Belting, M. Metastasis Stimulation by Hypoxia and Acidosis-Induced Extracellular Lipid Uptake Is Mediated by Proteoglycan-Dependent Endocytosis. *Cancer Res.* **2016**, *76* (16), 4828−40.
(12) Giampietri, C.; Petrungaro, S.; Cordella, M.; Tabolacci, C.; Tomaipitinca, L.; Facchiano, A.; Eramo, A.; Filippini, A.; Facchiano, F.; Ziparo, E., Lipid Storage and Autophagy in Melanoma Cancer Cells. *Int. J. Mol. Sci.* **2017**, *18*, (12).127110.3390/ijms18061271
(13) Rappa, G.; Fargeas, C. A.; Le, T. T.; Corbeil, D.; Lorico, A. Letter to the editor: An intriguing relationship between lipid droplets, cholesterol-binding protein CD133 and Wnt/beta-catenin signaling pathway in carcinogenesis. *Stem Cells* **2015**, *33* (4), 1366−70.
(14) Rappa, G.; Mercapide, J.; Anzanello, F.; Le, T. T.; Johlfs, M. G.; Fiscus, R. R.; Wilsch-Bräuninger, M.; Corbeil, D.; Lorico, A. Wnt Interaction and extracellular release of prominin-1/CD133 in human malignant melanoma cells. *Exp. Cell Res.* **2013**, *319* (6), 810−819.
(15) Qiu, B.; Ackerman, D.; Sanchez, D. J.; Li, B.; Ochocki, J. D.; Grazioli, A.; Bobrovnikova-Marjon, E.; Diehl, J. A.; Keith, B.; Simon, M. C. HIF-2α dependent lipid storage promotes endoplasmic reticulum homeostasis in clear cell renal cell carcinoma. *Cancer Discovery* **2015**, *5* (6), 652−667.
(16) Al-Zoughbi, W.; Pichler, M.; Gorkiewicz, G.; Guertl-Lackner, B.; Haybaeck, J.; Jahn, S. W.; Lackner, C.; Liegl-Atzwanger, B.; Popper, H.; Schauer, S.; Nusshold, E.; Kindt, A. S.; Trajanoski, Z.; Speicher, M. R.; Haemmerle, G.; Zimmermann, R.; Zechner, R.; Vesely, P. W.; Hoefler, G. Loss of adipose triglyceride lipase is associated with human cancer and induces mouse pulmonary neoplasia. *Oncotarget* **2016**, *7* (23), 33832−40.
(17) Ong, K. T.; Mashek, M. T.; Bu, S. Y.; Greenberg, A. S.; Mashek, D. G. Adipose triglyceride lipase is a major hepatic lipase that regulates triacylglycerol turnover and fatty acid signaling and partitioning. *Hepatology* **2011**, *53* (1), 116−26.
(18) Kopp, F.; Komatsu, T.; Nomura, D. K.; Trauger, S. A.; Thomas, J. R.; Siuzdak, G.; Simon, G. M.; Cravatt, B. F. The glycerophospho metabolome and its influence on amino acid homeostasis revealed by brain metabolomics of GDE1(−/−) mice. *Chem. Biol.* **2010**, *17* (8), 831−40.
(19) Mulvihill, M. M.; Benjamin, D. I.; Ji, X.; Le Scolan, E.; Louie, S. M.; Shieh, A.; Green, M.; Narasimhalu, T.; Morris, P. J.; Luo, K.; Nomura, D. K. Metabolic profiling reveals PAFAH1B3 as a critical driver of breast cancer pathogenicity. *Chem. Biol.* **2014**, *21* (7), 831−40.
(20) Tyanova, S.; Temu, T.; Sinitcyn, P.; Carlson, A.; Hein, M. Y.; Geiger, T.; Mann, M.; Cox, J. The Perseus computational platform for comprehensive analysis of (prote)omics data. *Nat. Methods* **2016**, *13* (9), 731−40.
(21) Wisniewski, J. R.; Zougman, A.; Nagaraj, N.; Mann, M. Universal sample preparation method for proteome analysis. *Nat. Methods* **2009**, *6* (5), 359−62.
(22) Cox, J.; Mann, M. MaxQuant enables high peptide identification rates, individualized p.p.b.-range mass accuracies and proteome-wide protein quantification. *Nat. Biotechnol.* **2008**, *26* (12), 1367−72.
(23) Ward, J. H. Hierarchical Grouping to Optimize an Objective Function. *J. Am. Stat. Assoc.* **1963**, *58* (301), 236−244.
(24) Vizcaino, J. A.; Deutsch, E. W.; Wang, R.; Csordas, A.; Reisinger, F.; Rios, D.; Dianes, J. A.; Sun, Z.; Farrah, T.; Bandeira, N.; Binz, P. A.; Xenarios, I.; Eisenacher, M.; Mayer, G.; Gatto, L.; Campos, A.; Chalkley, R. J.; Kraus, H. J.; Albar, J. P.; Martinez-Bartolome, S.; Apweiler, R.; Omenn, G. S.; Martens, L.; Jones, A. R.; Hermjakob, H. ProteomeXchange provides globally coordinated proteomics data submission and dissemination. *Nat. Biotechnol.* **2014**, *32* (3), 223−6.
(25) Chu, V. T.; Weber, T.; Wefers, B.; Wurst, W.; Sander, S.; Rajewsky, K.; Kuhn, R. Increasing the efficiency of homology-directed repair for CRISPR-Cas9-induced precise gene editing in mammalian cells. *Nat. Biotechnol.* **2015**, *33* (5), 543−548.
(26) Lieber, M. R. The Mechanism of Double-Strand DNA Break Repair by the Nonhomologous DNA End Joining Pathway. *Annu. Rev. Biochem.* **2010**, *79*, 181−211.
(27) Bassa, B. V.; Noh, J. W.; Ganji, S. H.; Shin, M. K.; Roh, D. D.; Kamanna, V. S. Lysophosphatidylcholine stimulates EGF receptor activation and mesangial cell proliferation: regulatory role of Src and PKC. *Biochim. Biophys. Acta, Mol. Cell Biol. Lipids* **2007**, *1771* (11), 1364−71.
(28) Bassa, B. V.; Roh, D. D.; Vaziri, N. D.; Kirschenbaum, M. A.; Kamanna, V. S. Lysophosphatidylcholine activates mesangial cell PKC and MAP kinase by PLCgamma-1 and tyrosine kinase-Ras pathways. *Am. J. Physiol.* **1999**, *277* (3), F328−F337.
(29) Ishii, I.; Fukushima, N.; Ye, X.; Chun, J. Lysophospholipid receptors: signaling and biology. *Annu. Rev. Biochem.* **2004**, *73*, 321−54.
(30) Magnusson, C. D.; Haraldsson, G. G. Ether lipids. *Chem. Phys. Lipids* **2011**, *164* (5), 315−40.
(31) Cox, J.; Hein, M. Y.; Luber, C. A.; Paron, I.; Nagaraj, N.; Mann, M. Accurate proteome-wide label-free quantification by delayed normalization and maximal peptide ratio extraction, termed MaxLFQ. *Mol. Cell. Proteomics* **2014**, *13* (9), 2513−26.
(32) Parsons, S. J.; Parsons, J. T. Src family kinases, key regulators of signal transduction. *Oncogene* **2004**, *23* (48), 7906−9.
(33) Di Florio, A.; Capurso, G.; Milione, M.; Panzuto, F.; Geremia, R.; Fave, G. D.; Sette, C. Src family kinase activity regulates adhesion, spreading and migration of pancreatic endocrine tumour cells. *Endocr.-Relat. Cancer* **2007**, *14* (1), 111−124.
(34) King, S. J.; Nowak, K.; Suryavanshi, N.; Holt, I.; Shanahan, C. M.; Ridley, A. J. Nesprin-1 and nesprin-2 regulate endothelial cell shape and migration. *Cytoskeleton* **2014**, *71* (7), 423−34.
(35) Fallah-Tafti, A.; Foroumadi, A.; Tiwari, R.; Shirazi, A. N.; Hangauer, D. G.; Bu, Y.; Akbarzadeh, T.; Parang, K.; Shafiee, A. Thiazolyl N-benzyl-substituted acetamide derivatives: synthesis, Src

DOI: 10.1021/acs.jproteome.7b00782
J. Proteome Res. 2018, 17, 1415−1425

kinase inhibitory and anticancer activities. *Eur. J. Med. Chem.* **2011**, *46* (10), 4853−8.
(36) Schweiger, M.; Romauch, M.; Schreiber, R.; Grabner, G. F.; Hutter, S.; Kotzbeck, P.; Benedikt, P.; Eichmann, T. O.; Yamada, S.; Knittelfelder, O.; Diwoky, C.; Doler, C.; Mayer, N.; De Cecco, W.; Breinbauer, R.; Zimmermann, R.; Zechner, R. Pharmacological inhibition of adipose triglyceride lipase corrects high-fat diet-induced insulin resistance and hepatosteatosis in mice. *Nat. Commun.* **2017**, *8*, 14859.
(37) Nomura, D. K.; Long, J. Z.; Niessen, S.; Hoover, H. S.; Ng, S. W.; Cravatt, B. F. Monoacylglycerol lipase regulates a fatty acid network that promotes cancer pathogenesis. *Cell* **2010**, *140* (1), 49−61.
(38) Antalis, C. J.; Uchida, A.; Buhman, K. K.; Siddiqui, R. A. Migration of MDA-MB-231 breast cancer cells depends on the availability of exogenous lipids and cholesterol esterification. *Clin. Exp. Metastasis* **2011**, *28* (8), 733−41.
(39) Pascual, G.; Avgustinova, A.; Mejetta, S.; Martin, M.; Castellanos, A.; Attolini, C. S.; Berenguer, A.; Prats, N.; Toll, A.; Hueto, J. A.; Bescos, C.; Di Croce, L.; Benitah, S. A. Targeting metastasis-initiating cells through the fatty acid receptor CD36. *Nature* **2017**, *541* (7635), 41−45.
(40) Zagani, R.; El-Assaad, W.; Gamache, I.; Teodoro, J. G. Inhibition of adipose triglyceride lipase (ATGL) by the putative tumor suppressor G0S2 or a small molecule inhibitor attenuates the growth of cancer cells. *Oncotarget* **2015**, *6* (29), 28282−95.
(41) Irby, R. B.; Yeatman, T. J. Role of Src expression and activation in human cancer. *Oncogene* **2000**, *19* (49), 5636−42.
(42) Bailey, A. P.; Koster, G.; Guillermier, C.; Hirst, E. M.; MacRae, J. I.; Lechene, C. P.; Postle, A. D.; Gould, A. P. Antioxidant Role for Lipid Droplets in a Stem Cell Niche of Drosophila. *Cell* **2015**, *163* (2), 340−353.
(43) Herms, A.; Bosch, M.; Ariotti, N.; Reddy, B. J.; Fajardo, A.; Fernandez-Vidal, A.; Alvarez-Guaita, A.; Fernandez-Rojo, M. A.; Rentero, C.; Tebar, F.; Enrich, C.; Geli, M. I.; Parton, R. G.; Gross, S. P.; Pol, A. Cell-to-cell heterogeneity in lipid droplets suggests a mechanism to reduce lipotoxicity. *Curr. Biol.* **2013**, *23* (15), 1489−96.
(44) Listenberger, L. L.; Han, X.; Lewis, S. E.; Cases, S.; Farese, R. V., Jr.; Ory, D. S.; Schaffer, J. E. Triglyceride accumulation protects against fatty acid-induced lipotoxicity. *Proc. Natl. Acad. Sci. U. S. A.* **2003**, *100* (6), 3077−82.
(45) Nguyen, T. B.; Louie, S. M.; Daniele, J. R.; Tran, Q.; Dillin, A.; Zoncu, R.; Nomura, D. K.; Olzmann, J. A. DGAT1-Dependent Lipid Droplet Biogenesis Protects Mitochondrial Function during Starvation-Induced Autophagy. *Dev. Cell* **2017**, *42* (1), 9−21e5.
(46) Accioly, M. T.; Pacheco, P.; Maya-Monteiro, C. M.; Carrossini, N.; Robbs, B. K.; Oliveira, S. S.; Kaufmann, C.; Morgado-Diaz, J. A.; Bozza, P. T.; Viola, J. P. Lipid bodies are reservoirs of cyclooxygenase-2 and sites of prostaglandin-E2 synthesis in colon cancer cells. *Cancer Res.* **2008**, *68* (6), 1732−40.
(47) Albert, D. H.; Anderson, C. E. Ether-linked glycerolipids in human brain tumors. *Lipids* **1977**, *12* (2), 188−92.
(48) Gwak, G. Y.; Yoon, J. H.; Lee, S. H.; Lee, S. M.; Lee, H. S.; Gores, G. J. Lysophosphatidylcholine suppresses apoptotic cell death by inducing cyclooxygenase-2 expression via a Raf-1 dependent mechanism in human cholangiocytes. *J. Cancer Res. Clin. Oncol.* **2006**, *132* (12), 771−9.
(49) Howard, B. V.; Morris, H. P.; Bailey, J. M. Ether-lipids, -glycerol phosphate dehydrogenase, and growth rate in tumors and cultured cells. *Cancer Res.* **1972**, *32* (7), 1533−8.
(50) Meyer zu Heringdorf, D.; Jakobs, K. H. Lysophospholipid receptors: signalling, pharmacology and regulation by lysophospholipid metabolism. *Biochim. Biophys. Acta, Biomembr.* **2007**, *1768* (4), 923−40.
(51) Piano, V.; Benjamin, D. I.; Valente, S.; Nenci, S.; Marrocco, B.; Mai, A.; Aliverti, A.; Nomura, D. K.; Mattevi, A. Discovery of Inhibitors for the Ether Lipid-Generating Enzyme AGPS as Anti-Cancer Agents. *ACS Chem. Biol.* **2015**, *10* (11), 2589−97.
(52) Tan, M.; Hao, F.; Xu, X.; Chisolm, G. M.; Cui, M. Z. Lysophosphatidylcholine activates a novel PKD2-mediated signaling pathway that controls monocyte migration. *Arterioscler., Thromb., Vasc. Biol.* **2009**, *29* (9), 1376−82.
(53) Roos, D. S.; Choppin, P. W. Tumorigenicity of cell lines with altered lipid composition. *Proc. Natl. Acad. Sci. U. S. A.* **1984**, *81* (23), 7622−6.
(54) Kabarowski, J. H. G2A and LPC: regulatory functions in immunity. *Prostaglandins Other Lipid Mediators* **2009**, *89* (3−4), 73−81.
(55) Lan, W.; Yamaguchi, S.; Yamamoto, T.; Yamahira, S.; Tan, M.; Murakami, N.; Zhang, J.; Nakamura, M.; Nagamune, T. Visualization of the pH-dependent dynamic distribution of G2A in living cells. *FASEB J.* **2014**, *28* (9), 3965−74.
(56) Koizume, S.; Miyagi, M. Lipid Droplets: A Key Cellular Organelle Associated with Cancer Cell Survival under Normoxia and Hypoxia. *Int. J. Mol. Sci.* **2016**, *17* (9), E1430.
(57) Abramczyk, H.; Surmacki, J.; Kopec, M.; Olejnik, A. K.; Lubecka-Pietruszewska, K.; Fabianowska-Majewska, K. The role of lipid droplets and adipocytes in cancer. Raman imaging of cell cultures: MCF10A, MCF7, and MDA-MB-231 compared to adipocytes in cancerous human breast tissue. *Analyst* **2015**, *140* (7), 2224−35.

DOI: 10.1021/acs.jproteome.7b00782
J. Proteome Res. 2018, 17, 1415−1425